ÓPTICA PURA Y APLICADA
www.sedoptica.es

Type: RESEARCH PAPER

Non-paraxial focusing by microlenses under arbitrary spatial coherence

Enfoque no paraxial mediante microlentes bajo coherencia espacial arbitraria

Rafael A. Casalins-Hernández[1,*], Román Castañeda[1,S]

1. Physics Department, Universidad Nacional de Colombia Sede Medellín, A.A. 3840, Medellín, Colombia

(*)E-mail: rcasalins@unal.edu.co S: miembro de SEDOPTICA / SEDOPTICA member

Received: 28/8/2025 Accepted: 15/2/2026
DOI: 10.7149/OPA.59.1.51225

ABSTRACT:

Non-paraxial focusing of monochromatic optical fields under arbitrary spatial coherence by spherical microlenses is theoretically discussed and numerically analyzed. A 3D concentration of the power spectrum determines the focal volume, which has rotation symmetry around the optical axis and whose maximum is corresponding to the focal point. A quantitative descriptor is introduced for characterizing the focal volume under different conditions, such as transverse illumination area on the lens, focal depth, radii of the spherical surfaces and spatial coherence of the illumination.

Key words: microlens, nanolens, focusing, partially coherent light, non-paraxial propagation

RESUMEN:

Se discute teóricamente y se analiza numéricamente el enfoque no paraxial de campos ópticos monocromáticos bajo coherencia espacial arbitraria mediante microlentes esféricas. Una concentración tridimensional del espectro de potencia determina el volumen focal, que tiene simetría de rotación alrededor del eje óptico y cuyo máximo corresponde al punto focal. Se introduce un descriptor cuantitativo para caracterizar el volumen focal en diferentes condiciones, tales como el área de iluminación sobre la lente, el diámetro transversal, la profundidad focal, los radios de las superficies esféricas y la coherencia espacial de la iluminación.

Palabras clave: microlentes, nanolentes, enfoque, luz parcialmente coherente, propagación no-paraxial

---

REFERENCES AND LINKS / REFERENCIAS Y ENLACES

[1] M. Born and E. Wolf, Principles of optics: electromagnetic theory of propagation, interference and diffraction of light (Elsevier, 2013).

[2] J. W. Goodman, Introduction to Fourier optics (Roberts and Company publishers, 2005).

[3] Y. Sung and C. J. Sheppard, "Three-dimensional imaging by partially coherent light under nonparaxial condition," Journal of the Optical Society of America A **28**(4), 554–559 (2011).

[4] N. I. Petrov, "Nonparaxial Focusing of Partially Coherent Gaussian Schell-Model and Bessel-Correlated Beams in Free Space," in Photonics, vol. 10, p. 857 (MDPI, 2023).

[5] J. C. Petruccelli, N. J. Moore, and M. A. Alonso, "Two methods for modeling the propagation of the coherence and polarization properties of nonparaxial fields," Optics communications **283**(22), 4457–4466 (2010).

[6] D. Weninger, C. Duessel, S. Serna, L. Kimerling, and A. Agarwal, "Graded index couplers for next generation chip-to-chip and fiber-to-chip photonic packaging," Journal of Physics: Photonics **8**(1), 015,005 (2026).

[7] R. Marchetti, C. Lacava, L. Carroll, K. Gradkowski, and P. Minzioni, "Coupling strategies for silicon photonics integrated chips," Photonics Research **7**(2), 201–239 (2019).

[8] R. Castañeda, J. Moreno, D. Colorado, and J. Laverde, "3D non-paraxial kernel for two-point correlation modelling in optical and quantum interference at the micro and nano-scales," Physica Scripta **95**(6), 065,502 (2020).

[9] R. Castañeda, J. Laverde, and J. Moreno, "Matrix algorithm for 3D nonparaxial optical field modeling under arbitrary spatial coherence," Applied Optics **59**(13), D21–D30 (2020).

[10] B. S. Luk'yanchuk, R. Paniagua-Domínguez, I. Minin, O. Minin, and Z. Wang, "Refractive index less than two: photonic nanojets yesterday, today and tomorrow," Optical Materials Express **7**(6), 1820–1847 (2017).

[11] M. Yousefi, T. Scharf, and M. Rossi, "Photonic nanojet generation under converging and diverging beams," Journal of the Optical Society of America B **38**(2), 317–326 (2021).

[12] Z. Wang and W. Zhang, "Sub-50 nm focusing of a 405 nm laser by hemispherical silicon nanolens," Journal of the Optical Society of America B **38**(1), 44–50 (2020).

[13] Y.-X. Ren, X. Zeng, L.-M. Zhou, C. Kong, H. Mao, C.-W. Qiu, K. K. Tsia, and K. K. Wong, "Photonic nanojet mediated backaction of dielectric microparticles," ACS Photonics **7**(6), 1483–1490 (2020).

1. Introduction

Focusing is the most important ability of a spherical lens. It is characterized by a significant concentration of the power spectrum in a small region behind the lens, called the focal point, when the lens is illuminated by a plane wavefront.

Paraxial focusing by thin spherical lenses is a well-established approximated model [1,2].Non-paraxial focusing of optical fields under arbitrary spatial coherence has been studied through different approximations, especially for Schell-Model and Bessel-Correlated beams [3–5]. However, the description of non-paraxial focusing of general optical fields by phase only optical elements remains necessary, in particular by spherical phase microelements, i.e. microlenses, which are potentially useful in micro-optics and integrated photonics applications [6, 7]. At this scale the spatial coherence state of the optical field should be considered.

With this aim, we use the exact non-paraxial model for optical field propagation reported in [8] and the numerical calculations follows the methodology detailed in [9]. We show that non-paraxial focusing determines focal volumes with more complex morphology than the focal volumes determined by the paraxial approached focusing [1]. In addition, we show that non-paraxial focusing characterization is challenging, because of its crucial dependence of parameters such as the spatial coherence degree of the optical field [1], the illumination cross-section, the radii of the spherical phase distribution and the microlens diameter.

2. Fundamentals

Let us consider the non-paraxial propagation of a quasi-monochromatic and linearly polarized optical field with arbitrary spatial coherence [8] in the volume delimited by the planes M and D separated at a distance z to each other as described in Fig. 1. Reduced coordinates ($\boldsymbol{\xi}_A$,$\boldsymbol{\xi}_D$) and ($\boldsymbol{r}_A$,$\boldsymbol{r}_D$) denote pairs of points at M and D respectively, with the coordinates suffixed A for the position of the midpoint between the pair and the coordinate suffixed D for the separation vector of the pair. So, pairs of points of M and D are determined by $\boldsymbol{\xi}_\pm = \boldsymbol{\xi}_A \pm \boldsymbol{\xi}_D/2$ and $\boldsymbol{r}_\pm = \boldsymbol{r}_A \pm \boldsymbol{r}_D/2$, respectively.

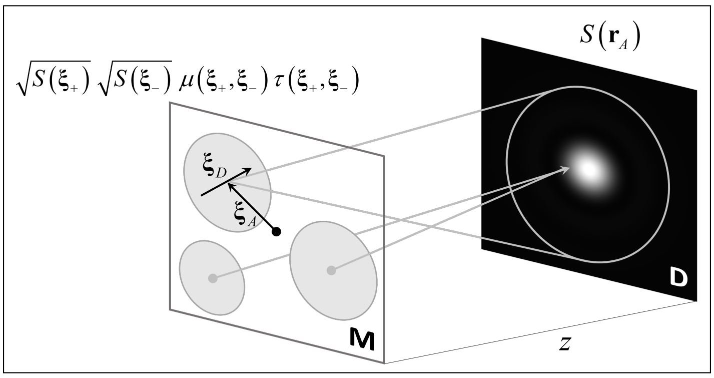

Fig. 1: Conceptual sketch of the non-paraxial propagation of quasi-monochromatic and linearly polarized optical fields with arbitrary spatial coherence, from M to D, and its square modulus detection at D. Shadowed circles at M represent structured supports of spatial coherence. Pairs of points within them are denoted by reduced coordinates $(\boldsymbol{\xi}_A, \boldsymbol{\xi}_D)$. Mathematical expressions are explained in the text.

The cross-spectral density $W(\boldsymbol{\xi}_+,\boldsymbol{\xi}_-) = \mu(\boldsymbol{\xi}_+,\boldsymbol{\xi}_-)\sqrt{S(\boldsymbol{\xi}_+)}\sqrt{S(\boldsymbol{\xi}_-)}$ describes the optical field at M, with $\mu(\boldsymbol{\xi}_+,\boldsymbol{\xi}_-)$ and $S(\boldsymbol{\xi}_\pm)$ its complex degree of spatial coherence and its power spectrum, respectively [1]. It should be noted that $\mu(\boldsymbol{\xi}_+,\boldsymbol{\xi}_-)=\mu^*(\boldsymbol{\xi}_-,\boldsymbol{\xi}_+)$, so that $W(\boldsymbol{\xi}_+,\boldsymbol{\xi}_-)=W^*(\boldsymbol{\xi}_-,\boldsymbol{\xi}_+)$, with the asterisk denoting complex conjugate. In addition, $\mu(\boldsymbol{\xi}_A,\boldsymbol{\xi}_A)=1$ and the area of pair of points $\boldsymbol{\xi}_\pm$, centered at any $\boldsymbol{\xi}_A$, outside which $\mu(\boldsymbol{\xi}_+,\boldsymbol{\xi}_-)$ takes on null or negligible values is called the structured support of spatial coherence at $\boldsymbol{\xi}_A$ (Fig. 1). The cross-spectral density that characterizes the optical field at D is given by

$$W(\boldsymbol{r}_+,\boldsymbol{r}_-)=\int_M\int_M d^2\boldsymbol{\xi}_A d^2\boldsymbol{\xi}_D W(\boldsymbol{\xi}_+,\boldsymbol{\xi}_-)\tau(\boldsymbol{\xi}_+,\boldsymbol{\xi}_-)\times\Phi(\boldsymbol{\xi}_+,\boldsymbol{\xi}_-,\boldsymbol{r}_+,\boldsymbol{r}_-),\tag{1}$$

where $\tau(\boldsymbol{\xi}_+,\boldsymbol{\xi}_-)=t(\boldsymbol{\xi}_+)t^*(\boldsymbol{\xi}_-)$ is the non-local transmission [8] at pairs of points of M, with $t(\boldsymbol{\xi}_\pm)=|t(\boldsymbol{\xi}_\pm)|exp(i\phi(\boldsymbol{\xi}_\pm))$ the complex transmission function of the optical device or component placed at M, and

$$\begin{aligned}&\Phi(\boldsymbol{\xi}_+,\boldsymbol{\xi}_-,\boldsymbol{r}_+,\boldsymbol{r}_-)=\\&\left(\frac{k}{4\pi}\right)^2\left(\frac{z+|z+\boldsymbol{r}_+-\boldsymbol{\xi}_+|}{|z+\boldsymbol{r}_+-\boldsymbol{\xi}_+|^2}\right)\left(\frac{z+|z+\boldsymbol{r}_--\boldsymbol{\xi}_-|}{|z+\boldsymbol{r}_--\boldsymbol{\xi}_-|^2}\right)\\&\times\exp\left(ik|z+\boldsymbol{r}_+-\boldsymbol{\xi}_+|-ik|z+\boldsymbol{r}_--\boldsymbol{\xi}_-|\right)\end{aligned}\tag{2}$$

is the exact kernel for non-paraxial propagation [8], with $k=2\pi/\lambda$ and λ the wavelength. It should be noted that $\Phi(\boldsymbol{\xi}_+,\boldsymbol{\xi}_-,\boldsymbol{r}_+,\boldsymbol{r}_-)=\Phi^*(\boldsymbol{\xi}_-,\boldsymbol{\xi}_+,\boldsymbol{r}_-,\boldsymbol{r}_+)$. Nevertheless, only the component for $\boldsymbol{r}_D=0$ of the cross-spectral density at D, called the power spectrum [1], is recordable by square modulus detectors, i.e. $W(\boldsymbol{r}_A,\boldsymbol{r}_A)=S(\boldsymbol{r}_A)$. In order to specify the effect of the spatial coherence at M on the power spectrum at D, it is useful to express it as (the complete deduction of Eqs. (3) to (5) is reported in [8])

$$S(\boldsymbol{r}_A)=S_R(\boldsymbol{r}_A)+S_G(\boldsymbol{r}_A)\tag{3}$$

with

$$S_R(\boldsymbol{r}_A)=\left(\frac{k}{4\pi}\right)^2\int_M d^2\boldsymbol{\xi}_A S(\boldsymbol{\xi}_A)|t(\boldsymbol{\xi}_A)|^2\times\left(\frac{z+|z+\boldsymbol{r}_A-\boldsymbol{\xi}_A|}{|z+\boldsymbol{r}_A-\boldsymbol{\xi}_A|^2}\right)^2,\tag{4}$$

the contribution provided by single points at M, which is independent of the spatial coherence, and

$$\begin{aligned}S_G(\boldsymbol{r}_A)=&\,2\left(\frac{k}{4\pi}\right)^2\int_M\int_{M,\boldsymbol{\xi}_D\neq0}d^2\boldsymbol{\xi}_A d^2\boldsymbol{\xi}_D|\mu(\boldsymbol{\xi}_+,\boldsymbol{\xi}_-)|\\&\times|t(\boldsymbol{\xi}_+)||t(\boldsymbol{\xi}_-)|\sqrt{S(\boldsymbol{\xi}_+)}\sqrt{S(\boldsymbol{\xi}_-)}\\&\times\left(\frac{z+|z+\boldsymbol{r}_A-\boldsymbol{\xi}_+|}{|z+\boldsymbol{r}_A-\boldsymbol{\xi}_+|^2}\right)\left(\frac{z+|z+\boldsymbol{r}_A-\boldsymbol{\xi}_-|}{|z+\boldsymbol{r}_A-\boldsymbol{\xi}_-|^2}\right)\\&cos(k|z+\boldsymbol{r}_A-\boldsymbol{\xi}_+|-k|z+\boldsymbol{r}_A-\boldsymbol{\xi}_-|+\alpha(\boldsymbol{\xi}_+,\boldsymbol{\xi}_-)+\Delta\phi(\boldsymbol{\xi}_+,\boldsymbol{\xi}_-)),\end{aligned}\tag{5}$$

with $\Delta\phi(\boldsymbol{\xi}_+,\boldsymbol{\xi}_-)=\phi(\boldsymbol{\xi}_+)-\phi(\boldsymbol{\xi}_-)$, the contribution provided by pairs of points at M, which explicitly depend on the spatial coherence described by $\mu(\boldsymbol{\xi}_+,\boldsymbol{\xi}_-)=|\mu(\boldsymbol{\xi}_+,\boldsymbol{\xi}_-)|exp(i\alpha(\boldsymbol{\xi}_+,\boldsymbol{\xi}_-))$.

Now, let us consider a refractive spherical microlens placed at M in a medium of refractive index n_0. It is an optical device of refractive index n and size at micro or nano scale, delimited by spherical surfaces of radii R_1 and R_2 respectively, centered on the optical axis. The microlens thickness Δ_0 is the distance between its vertices [2]. Its exact transmission function

$$\begin{aligned}&t(\boldsymbol{\xi})=exp(ikn_0\Delta_0)\\&exp\left(ik(n-n_0)\left(-R_1\left(1-\sqrt{1-\frac{|\boldsymbol{\xi}|^2}{R_1^2}}\right)+R_2\left(1-\sqrt{1-\frac{|\boldsymbol{\xi}|^2}{R_2^2}}\right)\right)\right)\end{aligned}\tag{6}$$

characterizes this device as a phase-only optical element. So, the non-local transmission at M becomes

$$t_F(\boldsymbol{\xi}_+)t_F^*(\boldsymbol{\xi}_-) = exp\left(ik(n-n_0)\left(R_1\sqrt{1-\frac{|\boldsymbol{\xi}_+|^2}{R_1^2}} \right.\right. \\ \left.\left. -R_2\sqrt{1-\frac{|\boldsymbol{\xi}_+|^2}{R_2^2}} + R_2\sqrt{1-\frac{|\boldsymbol{\xi}_-|^2}{R_2^2}} - R_1\sqrt{1-\frac{|\boldsymbol{\xi}_-|^2}{R_1^2}} \right)\right), \tag{7}$$

and $|t(\boldsymbol{\xi}_A)|^2 = 1$ is the transmittance. Eqs. (3) to (7) constitute an exact description of the non-paraxial microlens behavior. It should be noted that only the component $S_G(\boldsymbol{r}_A)$ of the power spectrum $S(\boldsymbol{r}_A)$ is affected by the microlens as phase-only optical element. More precisely, the component $S_R(\boldsymbol{r}_A)$ is independent of the lens phase distribution, while the argument of the cosine factor in integrand of $S_G(\boldsymbol{r}_A)$ is affected by the lens phase distribution in Eq. (7). This means that the microlens acts on optical fields that are spatially coherent in some extent. Indeed, the power spectrum at D reduces to $S(\boldsymbol{r}_A) = S_R(\boldsymbol{r}_A)$ for spatially incoherent optical fields, i.e. $\mu(\boldsymbol{\xi}_+,\boldsymbol{\xi}_-) = 0$ for $\boldsymbol{\xi}_D = 0$.

3. Results and discussion

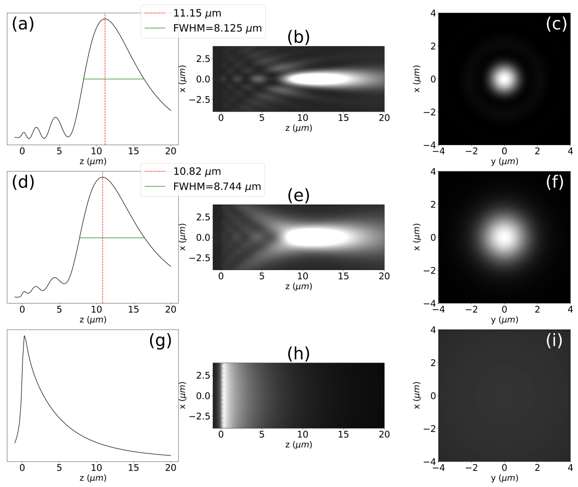

Fig. 2: Non-paraxial focusing provided by a microlens with $R_1 = -R_2 = 15\mu m$, $n = 1.5$, illuminated by wavefronts of $\lambda = 1.55\mu m$ in a medium of refractive index $n_0 = 1$. The left column shows the profiles along the z-axis, of the axial sections of the power spectrum distribution between M and D shown in the middle column. The main maximum position and axial Full Width at Half Maximum ($FWHM$) are indicated in the profiles on the left column. The right column shows the power spectrum distribution on the cross-section at the main maxima of the profiles on the right column.

The following numerical calculations and simulations were performed by applying the methodology reported in detail in [9]. So, it is not included here. Fig. 2 illustrates the exact non-paraxial focusing by a spherical microlens, which is illuminated by a uniform monochromatic wavefront of null phase with a Gaussian degree of spatial coherence. So, $S(\boldsymbol{\xi}_+) = S(\boldsymbol{\xi}_-) = S_0$, $|t(\boldsymbol{\xi}_+)| = |t(\boldsymbol{\xi}_-)| = 1$, $\alpha(\boldsymbol{\xi}_+,\boldsymbol{\xi}_-) = 0$ and $\mu(\boldsymbol{\xi}_+,\boldsymbol{\xi}_-) = exp(-|\boldsymbol{\xi}_D|^2/2\sigma^2)$, whose standard deviation σ determines the size of the structured supports of spatial coherence at M. Therefore, Eqs. (3) to (7) yield

$$S(\boldsymbol{r}_A) = \left(\frac{k}{4\pi}\right)^2 S_0 \left\{ \int_M d^2\boldsymbol{\xi}_A \left(\frac{z+|\boldsymbol{z}+\boldsymbol{r}_A-\boldsymbol{\xi}_A|}{|\boldsymbol{z}+\boldsymbol{r}_A-\boldsymbol{\xi}_A|^2} \right)^2 \right. \\ +2\int_M \int_{M,\boldsymbol{\xi}_D=0} d^2\boldsymbol{\xi}_A d^2\boldsymbol{\xi}_D \;\; exp(-|\boldsymbol{\xi}_D|^2/2\sigma^2) \\ \times \left(\frac{z+|\boldsymbol{z}+\boldsymbol{r}_A-\boldsymbol{\xi}_+|}{|\boldsymbol{z}+\boldsymbol{r}_A-\boldsymbol{\xi}_+|^2} \right) \left(\frac{z+|\boldsymbol{z}+\boldsymbol{r}_A-\boldsymbol{\xi}_-|}{|\boldsymbol{z}+\boldsymbol{r}_A-\boldsymbol{\xi}_-|^2} \right) \\ \left. cos(k|\boldsymbol{z}+\boldsymbol{r}_A-\boldsymbol{\xi}_+| - k|\boldsymbol{z}+\boldsymbol{r}_A-\boldsymbol{\xi}_-| + \Delta\phi(\boldsymbol{\xi}_+,\boldsymbol{\xi}_-)) \right\}, \tag{8}$$

for the power spectrum at D, with $\Delta\phi(\boldsymbol{\xi}_+,\boldsymbol{\xi}_-)$ determined by the exponent of Eq. (7). Equation (8) provides the images in Fig. 2 by adjusting the size of the spatial coherence support, by manipulating the standard deviation. Due to microlens non-linear phase, the power spectrum of the fully or partially coherent optical fields concentrates into a finite 3D region behind M, with rotation symmetric cross-section and axial spreading with a highly contrasted main maximum, placed at a distance comparable with the wavelength. The axial section of the power spectrum distribution is not symmetric with respect to the main maximum, and oscillates with relatively small secondary maxima before the main maximum. Such oscillations are absent behind the focal volume. It is illustrated in Fig. 2 top and middle rows for full spatial coherence (standard deviation significantly longer that the microlens cross-section diameter d, see Fig. 4) and partial coherence (standard deviation slightly shorter than d), respectively. The 3D region is not formed under full spatial incoherence, as illustrated on the bottom row for σ-to-d ratio of the order 10^{-5}.

Power spectrum concentration in this 3D region characterizes the non-paraxial (exact) microlens focusing, and the volume occupied by its main maximum is called the focal volume (it is also referred as photonic nano-jet [10–13]). The position of the power spectrum main maximum in the focal volume specifies the focal point and the axial Full Width at Half Maximum (FWHM) determines the focal depth. It is apparent in Fig. 2 that the spatial coherence reduction brings the following consequences on the focal volume: the focal length shortening, the focal depth increasing, the reduction of the power spectrum at the focal point, and the spreading of the power spectrum on the cross-section at the focal point. In other words, the focusing ability of phase-only microlenses reduces and eventually disappears as the spatial coherence of the optical field diminishes.

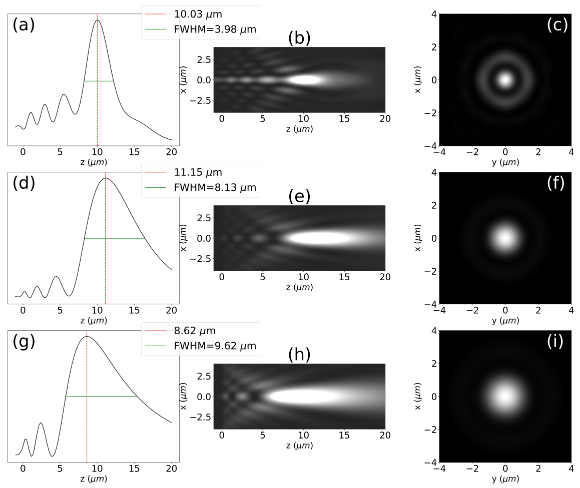

Fig. 3: Non-paraxial focusing provided by a microlens with $R_1 = -R_2 = 15\mu m$, illuminated by wavefronts of $\lambda = 1.55\mu m$, whose area covers: (i) the entire microlens (top row), (ii) the central half of the lens cross-section diameter (middle row), and (iii) the central third of the lens cross-section diameter (bottom row). Left column shows the z-profiles of the axial-section focal volumes shown in middle column. Right column shows the cross-sections of the volumes at the focal point. Focal point position and axial FWHM are indicated on the profiles.

Non-paraxial focusing strongly depends on microlens geometric features such as size of the illuminated area in the cross-section of the lens, the transverse diameter of the lens d and the radii of the spherical surfaces. Without loss of generality, let us analyze such features by considering the focusing of monochromatic, uniform and spatially coherent plane wavefront of null-phase that illuminate the microlenses. For illustration purposes, let us assume $n = 1.5$ for the microlenses and $n_0 = 1$ for the medium.

In Fig. 3, the wavefront illuminates transverse areas of different diameters on the microlens, so that a non-linear growth of $\Delta\phi(\boldsymbol{\xi}_+,\boldsymbol{\xi}_-)$ occurs as the illumination area increases. This brings the following consequences on the focal volume: focal depth shortening, increasing of the number and intensity of the secondary maxima, and their contrast reduction. The power spectrum distribution on the cross-section at the focal point consists of a central disc surrounded by rings. The smallest disc surrounded by a visible ring is obtained by illuminating completely the microlens (top row). The disc size increases and the ring contrast diminishes as the illumination area on the microlens cross-section reduces (middle and bottom rows).

Furthermore, focal length, focal depth and number of secondary maxima increase as the size of the microlens cross-section d grows. It is worth noting that the focal point is closely near to M for microlenses with d comparable with the wavelength. These features are illustrated in Fig. 4.

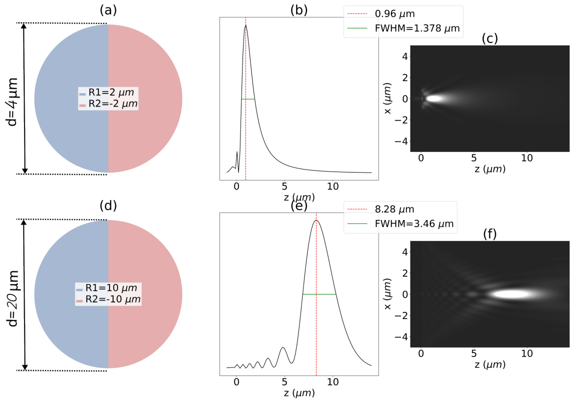

Fig. 4: Non-paraxial focusing provided by microlenses of different diameters, illuminated by wavefronts of $\lambda = 0.55\mu m$. Left column depicts the axial-sections of the lenses. Middle column shows the z- profiles of the axial-section focal volumes shown in right column. Focal point position and axial FWHM are indicated on the profiles.

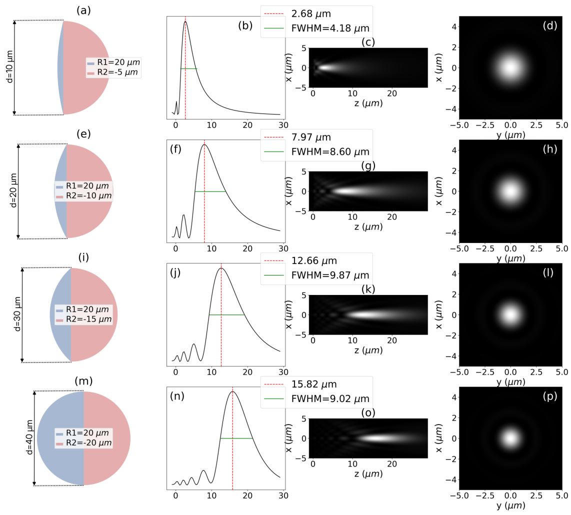

Fig. 5: Non-paraxial focusing by microlenses illuminated by wavefronts of $\lambda = 1.55\mu m$. The diameter of the illuminated transverse area is a half of d.. Left column depicts the axial-sections of the lenses. Second column from the left shows the z-profiles of the axial-section focal volumes shown in third column. Right column shows the cross-sections of the volumes at the focal point. Focal point position and axial FWHM are indicated on the profiles.

Microlenses with $R_1 \neq R_2$ are bilateral devices. This means that Eq. (7) remains invariant under the permutation $R_1 \leftrightarrow R_2$, so that non-paraxial focusing is unchanged as the order of the microlens surfaces is inverted. In addition, focal length shortens as one of the radii tends to infinity (i.e. the corresponding surface becomes a plane) and becomes maximum when both radii have the same length. It is illustrated in Fig. 5, where $R_1 >> -R_2$ on the top row, and $R_1 = -R_2$ on the bottom row.

Cross-sections of the focal volumes at several axial distances, provided by different microlenses are illustrated in Fig. 6. Power spectrum concentrates within central discs at the focal point, but spreads out on a rotation symmetric and concentric ring structure before the focal point and maintaining the central disc spot behind the focal point.

The visibility of the focal volume can be quantitatively estimated by a descriptor, independent of the illuminating intensity, defined as

$$\rho = \frac{T_{FWHM}}{A_{FWHM}}, \tag{9}$$

with T_{FWHM} and A_{FWHM} the transverse FWHM at the focal point and the axial FWHM on the z-axis respectively. From the qualitative analysis above is clear that $T_{FWHM} < A_{FWHM}$, so that $0 < \rho < 1$. Accordingly, $\rho \to 1$ when $A_{FWHM} \to T_{FWHM}$, thus denoting that the power spectrum is concentrated in a relatively small quasiellipsoid

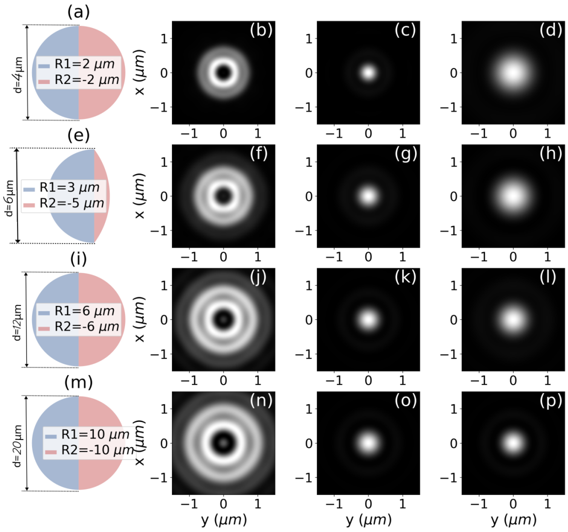

Fig. 6: Cross-sections of the non-paraxial focus volume provided by different microlenses illuminated by wavefronts of $\lambda = 0.55\mu m$ that cover a central transverse area of diameter equal to half d. Left column depicts the axial-sections of the lenses. Cross-sections (i) at the first minimum before the focal point (second column from the left), (ii) at the focal point (third column) and (iii) at a distance of $2\mu m$ beyond the focal point (right column).

volume with a visible focus point and a well-determined focus depth (Figs. 3 and 5). For $T_{FWHM} << A_{FWHM}$ then $\rho \rightarrow 0$ so that the power spectrum is not concentrated within a delimited volume beyond M plane. For this reason, ρ quantifies the non-paraxial focusing strength of the microlens.

Table 1 shows the non-paraxial focusing strength ρ of microlenses of different shapes, focal lengths and depths, illuminated with optical fields of specific wavelengths and Gaussian spatial coherence, whose structured support of spatial coherence is determined by the standard deviation σ. The transverse illumination area is considered too.

Table 1: Descriptors of non-paraxial focusing of different microlenses illuminated by spatially coherent Gaussian fields. $n = 1.5$ for the lens and $n_0 = 1$ for the medium.

(R_1, R_2) (μm)	λ (μm)	σ (μm)	Illumination area d (μm)	ρ	focal distance (μm)	focal depth (μm)
(20,–20)	1.55	∞	20	0.161	15.82	9.02
(20,–15)	1.55	∞	15	0.156	12.66	9.87
(20,–10)	1.55	∞	10	0.174	7.97	8.60
(20,–5)	1.55	∞	5	0.283	2.68	4.18
(15,–15)	1.55	∞	15	0.171	11.15	8.125
(15,–15)	1.55	R_1	15	0.271	10.82	8.744
(15,–15)	1.55	∞	10	0.185	8.62	9.62
(15,–15)	1.55	∞	30	0.210	10.03	3.98
(10,–10)	0.55	∞	10	0.157	8.28	3.46
(6,–6)	0.55	∞	6	0.166	4.60	3.02
(3,–5)	0.55	∞	3	0.196	2.11	2.46
(2,–2)	0.55	∞	2	0.289	0.96	1.378

4. Conclusions

We discussed an exact (non-paraxial) model for describing focusing by microlenses under arbitrary spatial coherence. At this scale, focusing is much more involved than the standard paraxial approximated description. The focal volume can be produced very near to the microlens and, in general its cross-section exhibits rotation symmetry with respect to the optical axis, while its axial-section is asymmetric with respect to the focal point (i.e. the point with the maximum power spectrum). Nevertheless, its morphology and focal length mainly depend on the spatial coherence, the geometry and transverse illumination area of the microlens, as characterized by ρ-parameter. The proposed model is a promising tool for designing and implementing devices for integrated optics and photonics.

Funding

Banco de la República de Colombia - Fundación para la promoción de la investigación y la tecnología (202517).

